

# Higher-order topology in monolayer graphene

Feng Liu<sup>\*1,2</sup> and Katsunori Wakabayashi<sup>†3,4</sup>

<sup>1</sup>School of Physical Science and Technology, Ningbo University, Ningbo, 315-211, China

<sup>2</sup>Laboratory of Clean Energy Storage and Conversion, Ningbo University, Ningbo, 315-211, China

<sup>3</sup>Department of Nanotechnology for Sustainable Energy, School of Science and Technology, Kwansei Gakuin University, Gakuen 2-1, Sanda 669-1337, Japan

<sup>4</sup>Center for Spintronics Research Network (CSRN), Osaka University, Toyonaka 560-8531, Japan

**We show that monolayer graphene intrinsically hosts higher-order topological corner states, in which electrons are localized topologically at atomic sizes. The emergence of the topological corner states in graphene is due to a non-trivial product of the Zak phases for two independent directions, which can be handily calculated graphically by using the bulk wavefunctions. We give an explicit expression that indicates the existence of topological corner states for various geometric edges and corner angles. We also demonstrate the nontrivial localization nature of the topological corner states in graphene by putting an imaginary onsite potential mask.**

---

<sup>\*</sup>LiuFeng@nbu.edu.cn

<sup>†</sup>waka@kwansei.ac.jp

The topology of energy bands has offered us a new dimension of designing solid-state materials with intriguing properties (*1*). One of the essential properties of topologically nontrivial systems is the bulk-edge correspondence, where robust edge and surface states appear at the interfaces which separate two topologically distinct systems (*2, 3*). These topological states are insensitive to the local perturbations that preserve the bulk topological invariants, also called topological protection. The recently proposed higher-order topology has extended such the bulk-edge correspondence to the more general bulk-edge-corner correspondence, where topological states of co-dimension larger than 1, i.e., topological corner states in two-dimensional systems, appear (*4, 5*). The higher-order topology has attracted significant attention in condensed matter physics, not only for its fundamental scientific importance but also because of its potential applications in electronics. In particular, topological corner states provide us the possibility of designing laser cavity and quantum computation with topological protection and maximized efficiency (*6–9*).

On the basis of several prototype models of higher-order topology, such as the two-dimensional Su-Schrieffer-Heeger model, the quadrupole insulator and the breathing Kagome lattice, non-trivial higher-order topology usually requires the fine-tuning of hopping textures plus external fields (*10–12*). Along this line, several proposals, such as monolayer graphdiyne (*13*), Kekulé-like lattice (*14*), twisted bilayer graphene (*15*), and topological insulators with the breaking of time-reversal symmetry (*16*), have been made. Unfortunately, the fine-tuning of hopping textures is difficult to realize in solid-state materials, as difficulties in the precise control of crystal growth. Besides the observation of the topological corner states in several artificial crystalline structures (*17–22*), the realization of higher-order topological states is remaining elusive in solid-state materials, especially in two-dimensions.

Without the fine-tuning of hopping textures or applying external fields, it is hard to imagine the emergence of higher-order topological states, especially in uniform systems. Motivated by a

simple picture that corners are “edges” of edges, we consider monolayer graphene as a possible candidate for topological corner states. Because in graphene, edge states accompanied with the perfectly conducting channel appear for various geometric ribbons only except for the armchair edge (23, 24). Later it was shown that the emergence of these edge states in graphene is due to a nonzero geometric phase – Zak phase (25). The Zak phase is a topological indicator for systems of zero Chern number that corresponds to the bulk charge polarization (26–29). Finite bulk charge polarization casts fractional surface charge on the direction perpendicular to the edges and results topological edge states (27). When the Zak phases in graphene along the two directions those are perpendicular to the edges forming the corner are both nontrivial, a corner state emerges.

We employ the tight-binding model with nearest-neighbor hoppings to describe the  $\pi$ -electronic states of graphene. The Hamiltonian for bulk graphene can be written as

$$H(\mathbf{k}) = -t|\rho(\mathbf{k})| \begin{pmatrix} 0 & e^{-i\phi(\mathbf{k})} \\ e^{i\phi(\mathbf{k})} & 0 \end{pmatrix} \quad (1)$$

in the basis of the two sublattices A and B as shown in Fig. 1A. Here,  $\rho(\mathbf{k}) = 1 + e^{-i\mathbf{k}\cdot\mathbf{a}_1} + e^{-i\mathbf{k}\cdot\mathbf{a}_2} \equiv |\rho(\mathbf{k})|e^{-i\phi(\mathbf{k})}$ .  $\mathbf{a}_1 = a(1/2, \sqrt{3}/2)$  and  $\mathbf{a}_2 = a(-1/2, \sqrt{3}/2)$  are the primitive vectors, where  $a = 2.46 \text{ \AA}$  is lattice constant of graphene.  $\mathbf{k} = (k_x, k_y)$  is the wavenumber vector.  $t = 2.75 \text{ eV}$  is the electron transfer integral between nearest-neighbor carbon atoms. The eigenenergies of bulk graphene are composed of two bands  $E_{\pm} = \pm t|\rho(\mathbf{k})|$ , and the corresponding eigen-wavefunctions are  $|u_{\mathbf{k}}, \pm\rangle = \frac{1}{\sqrt{2}}(e^{-i\phi(\mathbf{k})}, \pm 1)^T$ . For the valence band states  $|u_{\mathbf{k}}, -\rangle$ , the Zak phase along a specific direction  $\mathbf{i}$  is given as

$$Z_{\mathbf{i}}(k_{\mathbf{j}}) = \frac{1}{2} \int_{\mathbf{P}_{\mathbf{i}}(k_{\mathbf{j}})} \frac{d\phi(\mathbf{k})}{dk_{\mathbf{i}}} dk_{\mathbf{i}}, \quad (2)$$

where the direction  $\mathbf{j}$  is perpendicular to  $\mathbf{i}$ , and  $\mathbf{P}_{\mathbf{i}}(k_{\mathbf{j}})$  is a straight path connecting two equivalent  $k_{\mathbf{j}}$  points along  $\mathbf{i}$ . Because of the chiral symmetry, the value of Eq. (1) is either  $\pi$  or 0 in graphene. From Eq. (1) we see that  $Z_{\mathbf{i}}(k_{\mathbf{j}})$  is determined by the winding number of  $\phi(\mathbf{k})$  along

$\mathbf{P}_i(k_j)$ , which allows us to calculate Eq. (1) graphically through the density plot of  $\phi(\mathbf{k})$  as displayed in Fig. 1B. For a given  $k_j \in [-\pi/|\mathbf{T}|, \pi/|\mathbf{T}|]$  with that  $\mathbf{T}$  is the period of the graphene ribbon,  $Z_i(k_j) = \pi$  if  $\mathbf{P}_i(k_j)$  passes through the discontinuities of  $\phi(\mathbf{k})$ , and  $Z_i(k_j) = 0$  otherwise. For the typical zigzag ribbon, we have  $\mathbf{T} = \mathbf{a}_2$  and  $\mathbf{P}(0) = \mathbf{b}_1$  with  $\mathbf{b}_i \cdot \mathbf{a}_j = 2\pi\delta_{ij}$ , as shown in Fig. 1B. For other geometric ribbons, we have that  $\mathbf{T} \times \mathbf{P} = \mathbf{b}_1 \times \mathbf{b}_2$  in general. By fixing the gauge, let  $\mathbf{T}$  be evenly split by the  $\Gamma$  point, as in Fig. 1B. Through Fig. 1B we see that the Zak phase is  $\pi$  for  $\frac{2\pi}{3} < |k_j| \leq \pi$  of the zigzag ribbon, consistent with the energy band structure of the zigzag ribbon and the numerical calculation of the Zak phase along  $\mathbf{b}_1$  direction as displayed in Fig. 1C. The inset of Fig. 1C displays a zigzag edge with  $\mathbf{T} = \mathbf{a}_2$ . Nonzero  $Z_i(k_j)$  yields an imaginary solution  $k_i = \pi + i\eta_i$  at a specific  $k_j$ 's range for the boundary condition, e.g.,  $\sin(k_i N) + 2 \cos(k_j/2) \sin[k_i(N+1)] = 0$  for a width- $N$  zigzag ribbon, where  $\eta_i$  is the inverse of the localization length of the edge state (25, 30). Equation (2) describes the first-order topology of graphene.

For the second-order topology of graphene, we introduce the Zak phase  $Z_m(k_n)$  along another direction  $\mathbf{m}$ , where the two edges those are periodic along  $\mathbf{n}$  and  $\mathbf{j}$  forming the corner with an angle  $\theta$ . The emergence of a topological corner state suggests an exponentially localized solution along  $\mathbf{i}$  and  $\mathbf{m}$ , which requires that both  $Z_i(k_j)$  and  $Z_m(k_n)$  are nontrivial. This yields a twisted topological structure in momentum space associated with the corner angle  $\theta$ . Without losing generalities, we set  $Z_i$  as nontrivial, and we have  $k_i = \pi + i\eta_i$  for the corresponding  $k_j$ 's. Then according to the corner angle, we have  $k_n = \pi \sin \theta + k_j' \cos \theta$ . If  $k_n \in k_n'$ s those give nonzero  $Z_m$ , the topological corner state appears in graphene. In a compact form, such the twisted higher-order topological structure in momentum space can be presented as

$$Z_{\mathbf{im}}^\theta = \bigvee_{k_j > 0} \frac{Z_i(k_j) Z_m(k_j \cos \theta + \pi \sin \theta)}{\pi^2}, \quad (3)$$

where  $\bigvee_{k_j > 0}$  indicates taking the logical “or” for all possible  $k_j > 0$  within the 1st Brillouin zone.

Equation (3) involves two directions of the Zak phases with a twisted angle  $\theta$  that describes the second-order topology of graphene. When  $Z_{\text{im}}^\theta$  is not zero, a solution of  $\mathbf{k} = (\pi + i\eta_{\text{i}})\mathbf{i} + (\pi + i\eta_{\text{j}})\mathbf{j}$  exists.

For the demonstration of Eq. (3), we take the zigzag-zigzag corner as an example. There are two possible angles for the zigzag-zigzag corners, which are  $\pi/3$  and  $\pi/6$  (31). Topological corner states appear in the  $\pi/6$  zigzag-zigzag corners and are absent in the  $\pi/3$  corners, as displayed in Fig. 2A. The absence of the corner state in the  $\pi/3$  zigzag-zigzag corner is because for the  $\pi/3$  zigzag-zigzag corner, with a nontrivial Zak phase along  $\mathbf{i}$  the possible range of  $k_{\mathbf{n}}$  is determined by the corner angle  $\pi/3$  and  $k'_{\mathbf{j}} \in (2\pi/3, \pi]$  as

$$\begin{aligned} k_{\mathbf{n}} &\in \left[ \pi \cos \frac{\pi}{3} + \pi \sin \frac{\pi}{3}, \frac{2\pi}{3} \cos \frac{\pi}{3} + \pi \sin \frac{\pi}{3} \right) \\ &\approx [0.37\pi, 0.53\pi), \end{aligned} \quad (4)$$

which has no overlap with  $k'_{\mathbf{n}}$  range  $[-\pi, -2\pi/3) \cup (2\pi/3, \pi]$  for the nontrivial Zak phase along  $\mathbf{n}$ . This gives a trivial  $Z_{\text{im}}^\theta$  and suggests that it is impossible to take imaginary solutions of  $k_{\mathbf{m}}$  and  $k_{\mathbf{i}}$  simultaneously, and thus the corner state is absent in the  $\pi/3$  zigzag-zigzag corner. We replace one zigzag edge by the bearded edge in Fig. 2A, which has a complementary  $k'_{\mathbf{n}}$  range  $[-2\pi/3, 2\pi/3]$  to the zigzag ribbon, and we see that the topological corner states appear in the  $\pi/3$  zigzag-bearded corners as displayed in Fig. 2A.

Because of the chiral symmetry, the corner state in graphene is fixed at zero energy buried in the bulk and edge states, also called a bound state in continuum (32). To pick those corner states out, one possible way is to use a non-hermitian mask, i.e., an imaginary onsite potential  $\alpha = -0.005t$  in the diagonal terms of Eq. (1), indicted by the red shadow in Fig. 2A. With such the non-hermitian mask, only topological corner states remain non-decayed while the bulk and edge states fade out, because of the localization nature of the corner states. As displayed in Fig. 2B, the decaying rate of the topological corner state in the  $\pi/6$  zigzag-zigzag corner exponentially approaches to zero by increasing the area of the non-hermitian mask. From the

complex energy spectrum of the  $\pi/6$  zigzag-zigzag corner sample (upper panel of Fig. 2C), we see that except the topological corner states, other eigen-states all have finite decaying rates. In the  $\pi/3$  zigzag-zigzag corner sample, there is no non-decayed state due to the absence of topological corner states (lower panel of Fig. 2C). It is noted that except the armchair graphene ribbon, the Zak phase is always nonzero for a range of  $k'_j$ , and thus topological corner states exist for various edge shapes and corner angles in general.

At last, we emphasize that the emergence of topological corner states in graphene is due to the nontrivial Zak phases along two non-parallel directions. The perturbations those break the chiral symmetry such as the unsymmetric onsite potential and the real next-nearest-neighbor hopping would shift the eigenenergy of the corner state, and cannot suppress their existence as far as Eq. (3) remains nontrivial (33). As displayed in Fig. 3A and upper panel of Fig. 3B, with finite unsymmetric onsite potential, the topological corner state in the  $\pi/6$  zigzag-zigzag corner survives with a nonzero eigenenergy. For the finite real next-nearest-neighbor hopping, it renders the corner states with a longer decaying distance. Figure 3C displays the density of wavefunction of the corner states with next-nearest hopping  $0.1t$ . By increasing the size of the non-hermitian mask, we can confirm the localization nature of the corner state in Fig. 3C. As displayed in Fig. 3D, the imaginary part of eigenenergy of the corner state in Fig. 3C approaches exponentially to 0 with the size of the non-hermitian mask increasing. For the large spin-orbit coupling, it destroys the topological corner states in graphene, because a finite Chern number for a single spin channel breaks the monodromy of the Zak phase. For a single spin channel of graphene, the spin-orbit coupling can be simulated by the Haldane model (34, 35), where a finite imaginary next-nearest-neighbor hopping is assumed. As shown in lower panel of Fig. 3B, the complex energy spectrum of the  $\pi/6$  zigzag-zigzag corner sample with the non-hermitian mask and finite imaginary next-nearest-neighbor hopping, the non-decaying corner states are suppressed and a plateau of chiral edge states appear instead. It is fortunate that the spin-orbit

couplings are minimal in graphene, and we can neglect them safely.

To summarize, we have studied the higher-order topology of monolayer graphene. We have found that topological corner states exist in graphene for various geometric boundaries and corner angles. These topological corner states in graphene correspond to a twisted higher-order topological structure associated with the Zak phases in momentum space. Our results provide a possible way of localizing electrons at atomic sizes intrinsically in semi-metallic systems. Our predication is only based on monolayer graphene without substrate effects and the spin-orbit couplings, we believe that the experimental observation of topological corner states in graphene is possible.

## **Acknowledgments**

F.L. acknowledges the financial support by the Research Starting Funding of Ningbo University. K.W. acknowledges the financial support by JSPS KAKENHI Grant No. JP18H01154, and JST CREST Grant No. JPMJCR19T1.

## References

1. A. Bansil, H. Lin, T. Das, *Rev. Mod. Phys.* **88**, 021004 (2016).
2. Y. Hatsugai, *Phys. Rev. Lett.* **71**, 3697 (1993).
3. D. N. Sheng, Z. Y. Weng, L. Sheng, F. D. M. Haldane, *Phys. Rev. Lett.* **97**, 036808 (2006).
4. W. A. Benalcazar, B. A. Bernevig, T. L. Hughes, *Science* **357**, 61 (2017).
5. Z. Song, Z. Fang, C. Fang, *Phys. Rev. Lett.* **119**, 246402 (2017).
6. G. Harari, *et al.*, *Science* **359** (2018).
7. W. Zhang, *et al.*, *Light: Science & Applications* **9**, 109 (2020).
8. Y. Wu, H. Liu, J. Liu, H. Jiang, X. C. Xie, *National Science Review* **7**, 572 (2019).
9. Y. Wu, H. Jiang, J. Liu, H. Liu, X. C. Xie, *Phys. Rev. Lett.* **125**, 036801 (2020).
10. F. Liu, K. Wakabayashi, *Phys. Rev. Lett.* **118**, 076803 (2017).
11. W. A. Benalcazar, B. A. Bernevig, T. L. Hughes, *Phys. Rev. B* **96**, 245115 (2017).
12. M. Ezawa, *Phys. Rev. Lett.* **120**, 026801 (2018).
13. B. Liu, G. Zhao, Z. Liu, Z. F. Wang, *Nano Letters* **19**, 6492 (2019). PMID: 31393736.
14. F. Liu, H.-Y. Deng, K. Wakabayashi, *Phys. Rev. Lett.* **122**, 086804 (2019).
15. M. J. Park, Y. Kim, G. Y. Cho, S. Lee, *Phys. Rev. Lett.* **123**, 216803 (2019).
16. Y. Ren, Z. Qiao, Q. Niu, *Phys. Rev. Lett.* **124**, 166804 (2020).
17. M. Serra-Garcia, *et al.*, *Nature* **555**, 342 EP (2018).



18. C. W. Peterson, W. A. Benalcazar, T. L. Hughes, G. Bahl, *Nature* **555**, 346 EP (2018).
19. S. Imhof, *et al.*, *Nat. Phys.* **14**, 925 (2018).
20. Y. Ota, *et al.*, *Optica* **6**, 786 (2019).
21. H. Xue, *et al.*, *Nature Communications* **11**, 2442 (2020).
22. B. Xie, *et al.*, *Nature Communications* **11**, 3768 (2020).
23. K. Wakabayashi, Y. Takane, M. Yamamoto, M. Sigrist, *Carbon* **47**, 124 (2009).
24. A. R. Akhmerov, C. W. J. Beenakker, *Phys. Rev. B* **77**, 085423 (2008).
25. P. Delplace, D. Ullmo, G. Montambaux, *Phys. Rev. B* **84**, 195452 (2011).
26. J. Zak, *Phys. Rev. Lett.* **62**, 2747 (1989).
27. D. Vanderbilt, R. D. King-Smith, *Phys. Rev. B* **48**, 4442 (1993).
28. D. Obana, F. Liu, K. Wakabayashi, *Phys. Rev. B* **100**, 075437 (2019).
29. H. C. Wu, L. Jin, Z. Song, *Phys. Rev. B* **102**, 035145 (2020).
30. K. Wakabayashi, K. Sasaki, T. Nakanishi, T. Enoki, *Science and Technology of Advanced Materials* **11**, 054504 (2010).
31. Y. Shimomura, Y. Takane, K. Wakabayashi, *Journal of the Physical Society of Japan* **80**, 054710 (2011).
32. W. A. Benalcazar, A. Cerjan, *Phys. Rev. B* **101**, 161116 (2020).
33. C. Peng, R.-Q. He, Z.-Y. Lu, *Phys. Rev. B* **102**, 045110 (2020).
34. F. D. M. Haldane, *Phys. Rev. Lett.* **61**, 2015 (1988).

35. C. L. Kane, E. J. Mele, *Phys. Rev. Lett.* **95**, 226801 (2005).

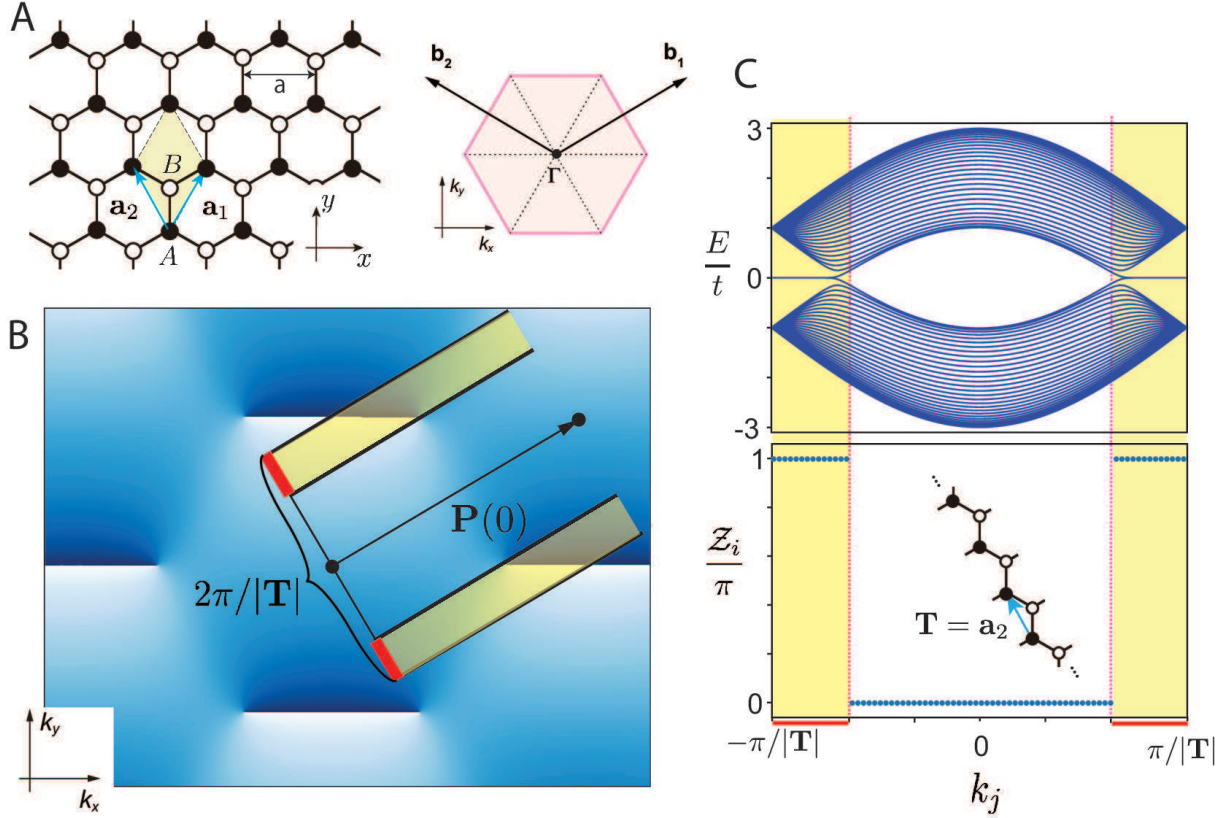


Figure 1: (A) (Left) Schematic of monolayer graphene with the primitive lattice vectors  $\mathbf{a}_1 = a(1/2, \sqrt{3}/2)$  and  $\mathbf{a}_2 = a(-1/2, \sqrt{3}/2)$ .  $a$  is the lattice constant of graphene. The yellow shade of rectangle indicates the unit cell. (Right) 1st Brillouin zone with the reciprocal primitive vectors  $\mathbf{b}_1 = \frac{2\pi}{a}(1, 1/\sqrt{3})$  and  $\mathbf{b}_2 = \frac{2\pi}{a}(-1, 1/\sqrt{3})$ . (B) Density plot of  $\phi(\mathbf{k})$  in the momentum space, where the black circles indicate the  $\Gamma$  point. For a graphene zigzag ribbon with the period  $\mathbf{T} = \mathbf{a}_2$ ,  $\mathcal{Z}(k) = \pi$  when the path  $\mathbf{P}(k)$  passes through the discontinuities of  $\phi(\mathbf{k})$ , as indicated by the red shades. (C) Energy band structure and numerical calculation of Zak phase for the zigzag graphene ribbon, where the nontrivial range (indicated by yellow shadow)  $k'_j$  is  $[-\pi, -2\pi/3) \cup (2\pi/3, \pi]$ . The width of zigzag ribbon is set as  $15\sqrt{3}a$ . Inset of (C) is the schematic of the graphene zigzag edge with the chosen unit cell in (A) and the period  $\mathbf{T} = \mathbf{a}_2$ .

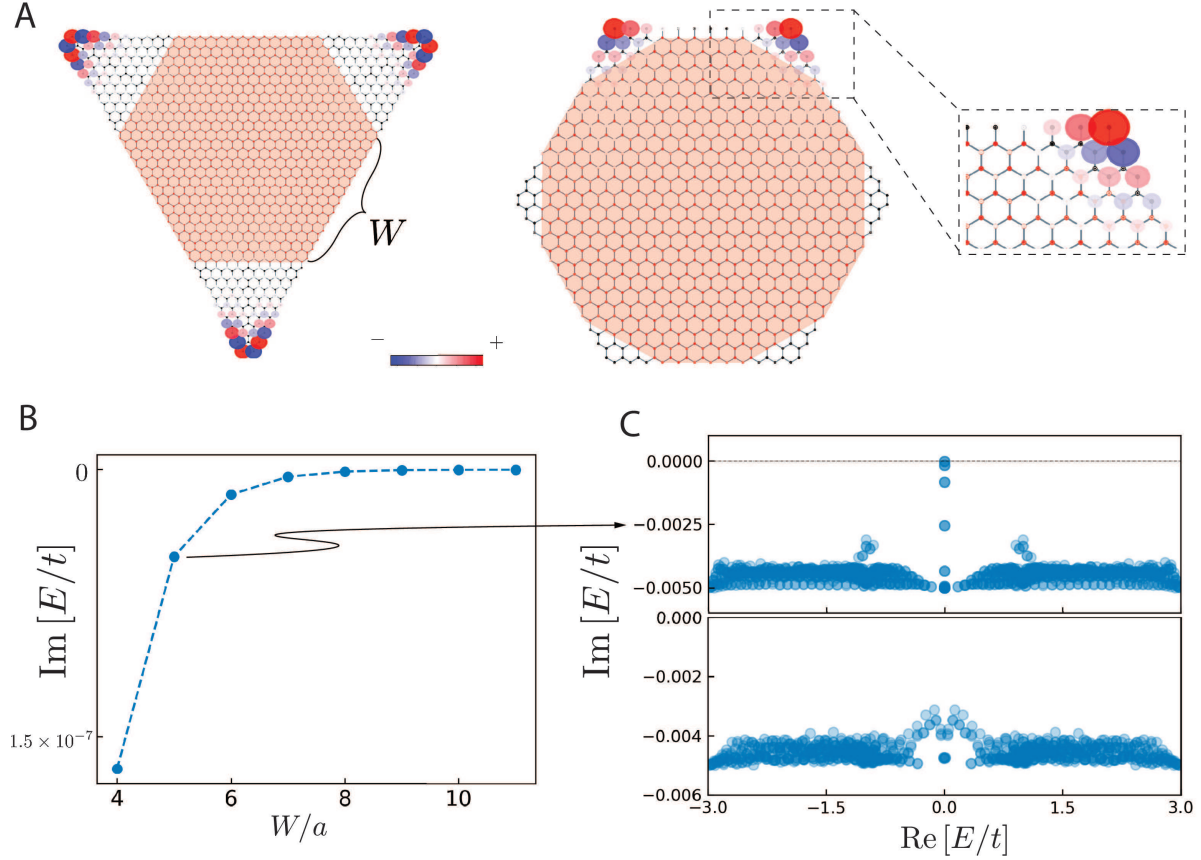


Figure 2: (A) Topological corner states of the  $\pi/6$  zigzag-zigzag corner and the  $\pi/3$  zigzag-bearded corner, where the size of circles indicates the local amplitude of the wavefunction, and blue and red indicate their signs. The red shade and sites in the middle parts indicate a non-hermitian mask where an imaginary onsite potential  $-0.005t$  is assumed. Inset shows a zoom of the topological corner state in the  $\pi/3$  zigzag-bearded corner. (B) Dependence of imaginary part of the eigenenergy for the topological corner state in the  $\pi/6$  zigzag-zigzag corner on the non-hermitian mask size  $W/a$ . By increasing the size of the non-hermitian mask, the imaginary part of the eigenenergy of the topological corner state in the  $\pi/6$  zigzag-zigzag corner approaches to zero exponentially. (C) Complex energy spectra of the  $\pi/6$  zigzag-zigzag corner sample for the non-hermitian mask size  $W/a = 5$  and the  $\pi/3$  zigzag-zigzag corner sample.

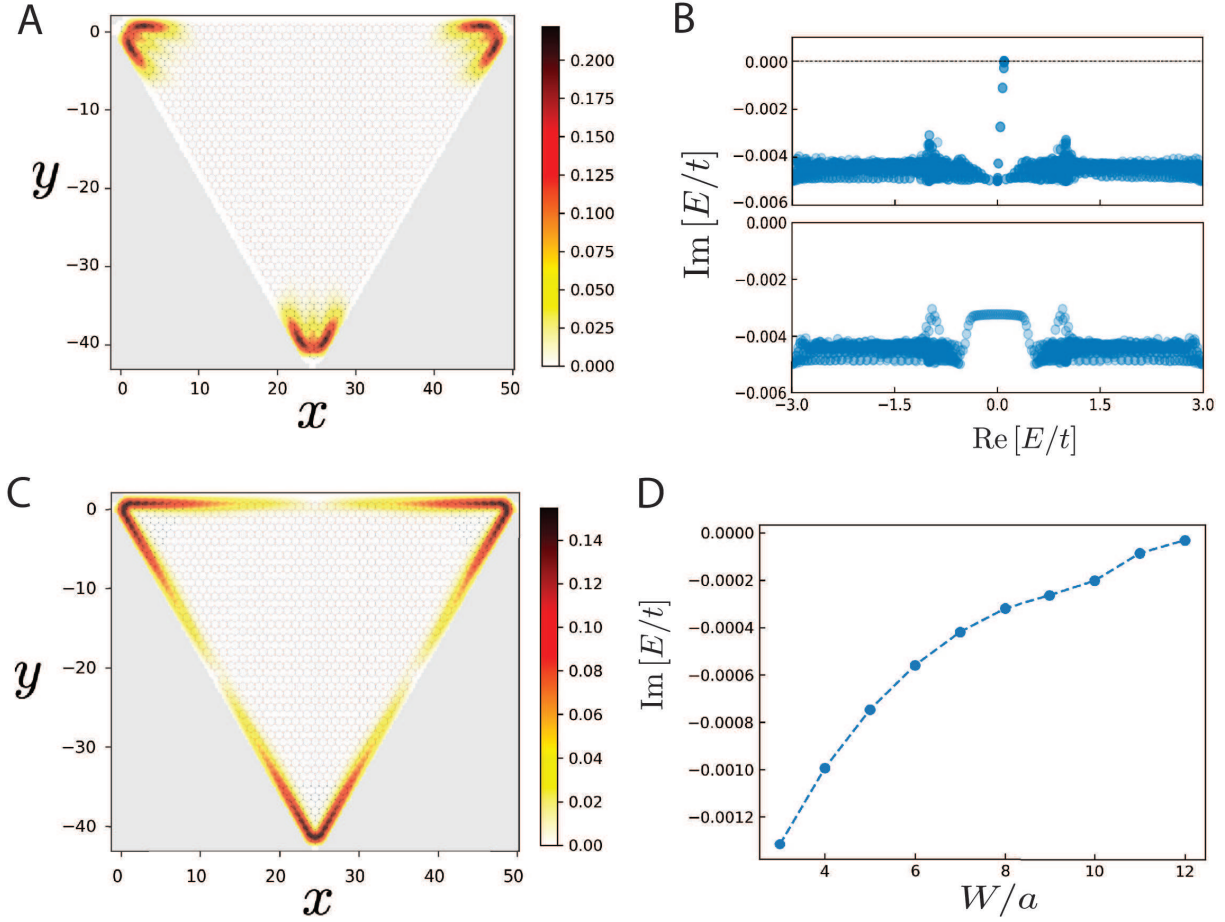


Figure 3: (A) Density of wavefunction for the topological corner state of  $\pi/6$  zigzag-zigzag corner with a unsymmetric onsite potential  $0.1$ . (B) Density of wavefunction for the topological corner state of  $\pi/6$  zigzag-zigzag corner with a next-nearest hopping  $0.1t$ . (C) Complex energy spectra of  $\pi/6$  zigzag-zigzag corner samples with a unsymmetric onsite potential  $0.1t$  (upper panel) and finite imaginary next-nearest-neighbor (lower panel). (D) Dependence of imaginary part of eigenenergy of the topological corner state in the  $\pi/6$  zigzag-zigzag corner with a real next-nearest hopping  $0.1$  on the size of the non-hermitian mask.